Solar Cells

DOI: 10.1002/anie.201308331

Sb_2Se_3-Sensitized Inorganic–Organic Heterojunction Solar Cells Fabricated Using a Single-Source Precursor**

*Yong Chan Choi, Tarak Nath Mandal, Woon Seok Yang, Yong Hui Lee, Sang Hyuk Im, Jun Hong Noh, and Sang Il Seok**

Abstract: *The photovoltaic performance of Sb_2Se_3-sensitized heterojunction solar cells, which were fabricated by a simple deposition of Sb_2Se_3 on mesoporous TiO_2 by an approach that features multiple cycles of spin coating with a single-source precursor solution and thermal decomposition, is reported. Poly[2,6-(4,4-bis(2-ethylhexyl)-4H-cyclopenta[2,1-b;3,4-b′]dithiophene)-alt-4,7(2,1,3-benzothioadiazole)] was used as the hole-transporting material. The most efficient cell exhibited a short-circuit current density of 22.3 mA cm^{-2}, an open-circuit voltage of 304.5 mV, and a fill factor of 47.2 %, yielding a power conversion efficiency of 3.21 % under standard test conditions (irradiation of 1000 W m^{-2}, air mass = 1.5 G). The results of this study imply that the developed approach has a high potential as a simple and effective route for the fabrication of efficient and inexpensive solar cells.*

Antimony trisulfide (stibnite, Sb_2S_3) has been widely used as a successful light sensitizer for efficient inorganic–organic heterojunction solar cells[1] because of its suitable band gap of approximately 1.7 eV and a high absorption coefficient of approximately 1.8×10^5 cm^{-1} at 450 nm.[2] We reported a power-conversion efficiency (PCE) of greater than 6% by employing appropriate hole-transporting materials (HTMs) that contain thiophene moieties[1b] and an additional electron channel.[1c] Although these Sb_2S_3-based solar cells have great potential, we faced difficulties in further improving PCE because of a limited charge contribution in the near-IR region[1c] and recombination pathways in Sb_2S_3.[3]

The use of antimony selenide (antimonselite, Sb_2Se_3) to replace Sb_2S_3 as a light sensitizer is one key strategy for achieving an enhanced efficiency in inorganic–organic heterojunction solar cells. Sb_2Se_3 displays a narrow band gap of 1.1–1.3 eV,[4] which approaches the ideal Shockley–Queisser value,[5] and has the ability to extend light harvesting over the near-IR region up to approximately 1000 nm. Theoretical calculations performed by Giustino et al.[4] demonstrated the improved performance of Sb_2Se_3-based devices compared to Sb_2S_3-cells, and suggested Sb_2Se_3 as a promising candidate for achieving 20% PCE. In spite of these in-depth studies, the photovoltaic performance of Sb_2Se_3-based solar cells has rarely been experimentally demonstrated thus far. Although photoelectrical solar cells using a Sb_2Se_3 photoanode that were fabricated by chemical bath deposition (CBD) were reported by Bhattacharya and co-workers,[6] the performance of these devices was very low (short-circuit photocurrent ca. 0.45 mA cm^{-2}; open-circuit photovoltage ca. 0.37 V). Guijarro et al. recently studied the charge dynamics of Sb_2Se_3-sensitized solar cells with 2,2′,7,7′-tetrakis(*N*,*N*-di-*para*-methoxyphenyl-amine)-9,9′-spirobifluorene as the HTM using transient absorption spectroscopy; however, the photovoltaic performance of these solar cells has not been reported to date.[7]

Chemical methods, such as CBD and successive ionic layer adsorption and reaction (SILAR), are widely employed for solar-cell fabrication. In the CBD method, Sb_2Se_3 is deposited in an aqueous solution that contains $SbCl_3$ and Na_2SeSO_3 as the antimony and selenium sources, respectively.[8] The major advantages of CBD are its simple process, versatile sources, and cost-effective instruments.[9] However, one notable drawback of this technique is the inevitable formation of precipitates or oxides, such as SbOCl, in the aqueous solution during Sb_2Se_3 synthesis, which results in unwanted impurities.[9,10] With the SILAR method, precipitate formation can be avoided through rinsing between immersion in the Sb precursor solution and immersion in the Se precursor solution.[7,9] Unfortunately, sodium-containing impurities such as Na_3SbSe_4 are easily formed during the heating step that is required for the crystallization of Sb_2Se_3, as sodium-based Se precursors are used in SILAR.[11] The design and development of a simple technique that is able to fabricate very pure Sb_2Se_3 is therefore important and pressing.

Herein, we describe an effective approach that is based on multiple cycles of spin coating of Sb_2Se_3 single-source precursor (Se-SSP) solutions followed by thermal decompo-

[*] Dr. Y. C. Choi, Dr. T. N. Mandal, W. S. Yang, Dr. Y. H. Lee, Dr. J. H. Noh, Prof. S. I. Seok
Division of Advanced Materials
Korea Research Institute of Chemical Technology (KRICT)
141 Gajeong-Ro, Yuseong-Gu, Daejeon 305-600 (Republic of Korea)
E-mail: seoksi@krict.re.kr
Prof. S. H. Im
Department of Chemical Engineering, Kyung Hee University
1 Seochon-dong, Giheung-gu, Youngin-si, Gyeonggi-do 446-701 (Republic of Korea)
Prof. S. I. Seok
Department of Energy Science, Sungkyunkwan University
Suwon 440-746 (Republic of Korea)
E-mail: seoksi@skku.edu

[**] This study was supported by the Global Research Laboratory (GRL) Program and the Global Frontier R&D Program on Center for Multiscale Energy System funded by the National Foundation under the Ministry of Science, ICT & Future, Korea, and by a grant from the KRICT 2020 Program for Future Technology of the Korea Research Institute of Chemical Technology (KRICT), Republic of Korea.

Supporting information for this article is available on the WWW under http://dx.doi.org/10.1002/anie.201308331.

sition for the deposition of Sb_2Se_3 on mesoporous TiO_2 (mp-TiO_2). We used a Se-SSP solution that comprises $[(SbL_2Cl_2)Cl]_2{\cdot}(CH_3)_2CO$, where L is *N*,*N*-dimethyl selenourea, which was newly synthesized by our group,[10] and the non-aqueous solvent *N*,*N*-dimethylformamide (DMF) to minimize the formation of impurities. Owing to the insoluble nature of the thermally decomposed residues in DMF, spin-coated Se-SSP accumulates after each cycle of thermal decomposition; therefore, we can control the amount of Sb_2Se_3 by choosing the appropriate number of cycles of spin coating and thermal decomposition. The morphology, elemental composition, absorption, and structure of the Sb_2Se_3 that was formed on mp-TiO_2 were investigated by field-emission scanning electron microscopy (FESEM), energy-dispersive X-ray (EDX) spectroscopy, UV/Vis spectroscopy, and X-ray diffraction (XRD), respectively. We then investigated the photovoltaic performance of the device that is based on Sb_2Se_3 as the light sensitizer and poly[2,6-(4,4-bis(2-ethylhexyl)-4*H*-cyclopenta[2,1-*b*;3,4-*b*′]dithiophene)-alt-4,7-(2,1,3-benzothiadiazole)] (PCPDTBT) as the HTM.

The fabrication process for Sb_2Se_3-sensitized inorganic–organic heterojunction solar cells is shown in Scheme 1. The

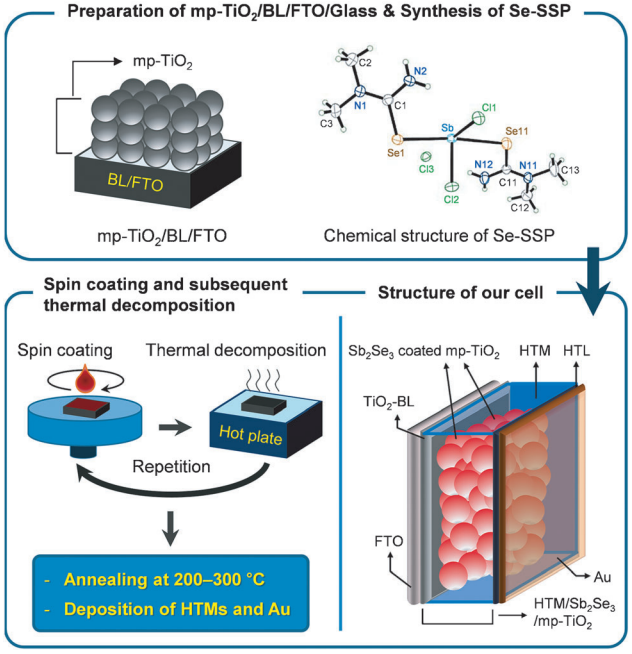

Scheme 1. Fabrication process for Sb_2Se_3-sensitized inorganic–organic heterojunction cells. Poly(3,4-ethylenedioxythiophene):poly(styrenesulfonate) (PEDOT:PSS) was used as the HTL.

process started with the preparation of 820 nm-thick mp-TiO_2 with approximately 50 nm particles on top of a 100 nm-thick compact TiO_2 blocking layer (TiO_2-BL)/F-doped SnO_2 (FTO; 8 $\Omega\,sq^{-1}$, Pilkington TEC-8).[1] The Se-SSP was synthesized according to procedures that we had previously developed.[12] The Se-SSP dissolved in DMF (0.01–0.2 $g\,mL^{-1}$) was spin-coated at 1000–3000 rpm for 60 seconds, which allowed the filling of Se-SSP into the mp-TiO_2 substrate. The Se-SSP/mp-TiO_2/TiO_2-BL/FTO was then thermally decomposed at 150–200 °C for two minutes in air, while the temperature was measured with a differential scanning calorimeter (see the Supporting Information, Figure S1). These cycles of spin coating and thermal decomposition were repeated, allowing for an accurate control of the Sb_2Se_3 deposition amount. Afterwards, the samples were annealed at 200–300 °C for five minutes in Ar atmosphere, which was followed by the deposition of the HTM and the gold electrode by spin coating and thermal evaporation, respectively.

To investigate the Se-SSP distribution in mp-TiO_2, we investigated morphology and elemental composition by FESEM equipped with an EDX spectrometer. Figure 1a

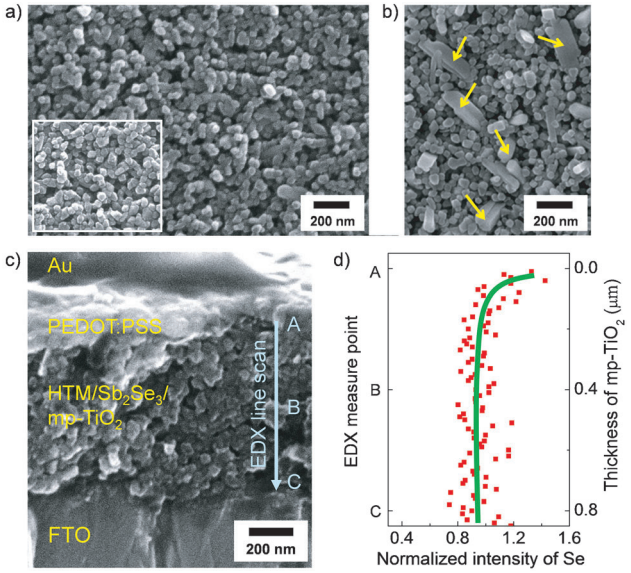

Figure 1. a, b) FESEM images showing the surface of Se-SSP-deposited mp-TiO_2 with Se-SSP concentrations of 0.05 $g\,mL^{-1}$ (a) and 0.2 $g\,mL^{-1}$ (b). The inset of (a) is a surface image of pure mp-TiO_2. c) Cross-sectional FESEM image of the final cells. d) EDX line scan profile. Antimony is excluded in the EDX analysis because the EDX energy of antimony (Lα: 3.604 keV) overlaps with that of tin (Lα: 3.443 keV, induced from FTO), and the peak intensity of antimony is rather low compared to that of tin.

shows a surface image of mp-TiO_2 after the deposition of Se-SSP that was obtained by FESEM spectroscopy. The Se-SSP was deposited by repeating 15 cycles of spin coating with a 0.05 $g\,mL^{-1}$ solution and thermal decomposition at 150 °C. The originally transparent mp-TiO_2 turned black after Se-SSP deposition, and except for its compositional particle sizes, its surface morphology was found to be similar to that of mp-TiO_2, which is a good indication of a uniform distribution of deposited Se-SSP on the mp-TiO_2 surface (Figure 1a). By carefully examining high-magnification images, we noticed that both the concentration of the SSP solution and the conditions for spin coating played significant roles in determining the surface morphology. An example of such a consequence is the presence of coarse nanorods (Figure 1b, →) that are spread over the entire surface when a SSP solution with a rather high concentration was used. The EDX line scan profile (Figure 1d) obtained from the cross-sectional FESEM

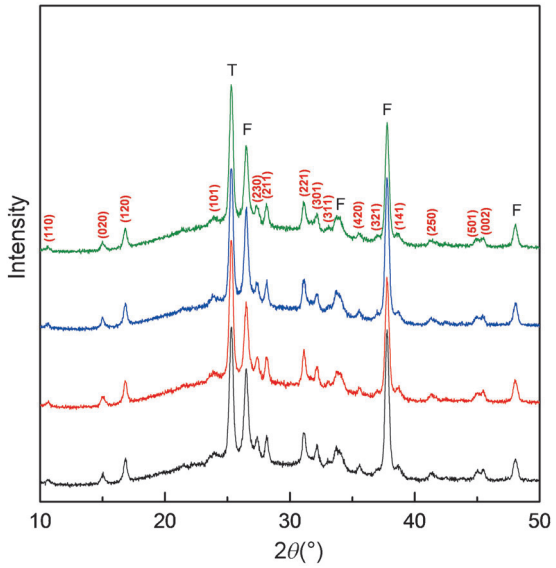

Figure 2. XRD patterns of Se-SSP-deposited mp-TiO_2/TiO_2-BL/FTO for different annealing temperatures. All of the samples were prepared by a multicyclic process of spin-coating with SSP solution (0.05 g mL^{-1}) and thermal decomposition at 150 °C, which was was repeated 15 times. NA (——): Se-SSP/mp-TiO_2/TiO_2-BL/FTO without annealing; A200–300: Se-SSP/mp-TiO_2/TiO_2-BL/FTO annealed at 200 °C (——), 250 °C (——), or 300 °C (——) under argon atmosphere. Peaks that can be attributed to TiO_2 and FTO are labelled T and F, respectively.

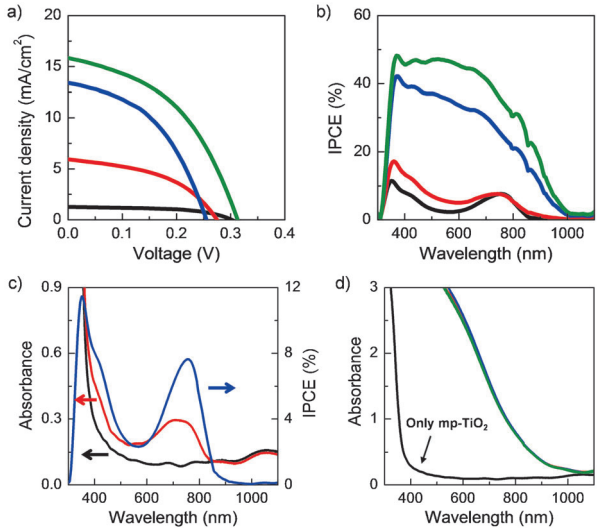

Figure 3. a) *J–V* curves and b) IPCE curves of cells that were prepared at different annealing temperatures. NA (——): Se-SSP/mp-TiO_2/TiO_2-BL/FTO without annealing; A200–300: Se-SSP/mp-TiO_2/TiO_2-BL/FTO annealed at 200 °C (——), 250 °C (——), or 300 °C (——). c) Comparison of the IPCE spectrum of a cell based on the NA sample (——) with the UV/Vis absorption spectra of mp-TiO_2/TiO_2-BL/FTO (——) and HTM/mp-TiO_2/TiO_2-BL/FTO (——). d) UV/Vis absorption spectra of NA (——), A200 (——), A250 (——), and A300 (——).

image (Figure 1c) of the cells reveals a deep penetration of Se-SSP into the 820 nm-thick mp-TiO_2, suggesting a homogeneous Se-SSP distribution throughout the mp-TiO_2 substrate.

XRD data of Se-SSP/mp-TiO_2/TiO_2-BL/FTO particles that were obtained with different annealing temperatures are shown in Figure 2. The Se-SSP/mp-TiO_2/TiO_2-BL/FTO was prepared by 15 cycles of spin coating and thermal decomposition under the same conditions as described above. The measured XRD pattern of the sample without annealing (NA) revealed 15 pronounced peaks (excluding those of TiO_2 and FTO), which were identified and labeled appropriately in terms of (*hkl*). These peaks were found to be well matched with the Sb_2Se_3 orthorhombic phases (JCPDS No. 15-0861), implying the absence of impurity phases, such as Sb_2O_3, in the processed substrate. Moreover, by adopting the same fabrication conditions as for the NA sample, Se-SSP deposition on glass also led to pure Sb_2Se_3 phases, as determined by XRD (Figure S2). With these results in hand, we concluded that the formation of a pure Sb_2Se_3 phase occurred shortly after thermal decomposition at a low temperature of approximately 150 °C. The significance of this finding is the possibility to synthesize low-temperature-processed Sb_2Se_3-based solar cells that are superior to conventional cells, which usually require annealing temperatures greater than 300 °C for crystallizing Sb_2Se_3. Accordingly, samples that were annealed at 200–300 °C (A200–A300, Figure 2) exhibited patterns with profiles that were identical to that of the NA sample, which suggests that the structure remains unchanged as the annealing temperature is increased to 200–300 °C.

The effect of the annealing temperature on the current density–voltage (*J–V*) curves and on the device parameters of

Table 1: Device parameters obtained from Figure 3a. All of the samples were measured at 98 mW cm^{-2}.

Sample	J_{SC} [mA cm^{-2}]	V_{OC} [mV]	*FF* [%]	PCE [%]
NA	1.3	302.9	55.1	0.22
A200	5.9	272.8	46.4	0.76
A250	13.4	252.6	45.4	1.57
A300	15.8	313.0	44.6	2.25

Sb_2Se_3-sensitized solar cells are shown in Figure 3a and Table 1, respectively. The Sb_2Se_3 that is studied in Figure 3 was deposited by twelve cycles of spin coating and thermal decomposition. PCPDTBT diluted in 1,2-dichlorobenzene (15 mg mL^{-1}) was used as the HTM. All devices were measured with the active area defined to be 0.096 cm^2 by using a metal mask. The device that was fabricated without annealing (device NA) exhibited a short-circuit current density (J_{SC}) of 1.3 mA cm^{-2}, an open-circuit voltage (V_{OC}) of 302 mV, and a fill factor (*FF*) of 55.1 %, which results in a PCE that approaches approximately 0.22 %. A significant improvement of the cell performance could be achieved by annealing at 200 °C, which led to a substantial increase in J_{SC} from 1.3 to 5.9 mA cm^{-2}; this parameter further increased to 15.8 mA cm^{-2} as the annealing temperature was increased to 300 °C, which corresponds to an improved PCE of 2.25 %. The incident photon to current efficiency (IPCE) spectra (Figure 3b) follow similar variations with changes of J_{SC}. This phenomenon can be used to infer that the HTM mainly contributes to the IPCE spectrum of the NA sample because the absorption band of the HTM matches the IPCE spectrum precisely[1c] (Figure 3c).

The IPCE is dependent on the light-harvesting efficiency, the efficiency of electron injection into TiO_2, and the charge-collection efficiency. In all of the cases that are discussed herein, Sb_2Se_3-deposited samples showed relatively invariable absorption properties with a band gap of approximately 1.2 eV, regardless of the diverse annealing conditions (Figure 3d). By taking this fact into account, a relatively low IPCE, which is closely related to the overall low J_{SC} values that were observed for samples of NA, A200, and A250, can be attributed to a low electron-injection yield. This could be due to the incomplete decomposition of residues from Se-SSP in these samples. To verify this assumption, elemental analysis of the Se-SSP for samples with different annealing temperatures was carried out. Table 2 reveals that the amount of the three elements carbon, hydrogen, and nitrogen gradually decreased to zero as the annealing temperature is increased to 300 °C, which is a good indication that the carbon-, hydrogen- and nitrogen-containing residues predominantly remain in the sample below 300 °C. TGA data of Sb_2Se_3-SSP (Figure S1a and Table S1) also confirmed the need for a complete removal of the residues from Se-SSP by post-annealing at approximately 300 °C; in the present study, this is supposed to be a prerequisite for highly efficient Sb_2Se_3-based solar cells.

Table 2: Elemental analysis for carbon, hydrogen, and nitrogen in the Se-SSP at different post-annealing temperatures.

T [°C]	Carbon	Hydrogen	Nitrogen
no annealing	12.95	3.02	10.27
150	12.10	2.86	9.69
200	7.21	2.06	5.82
300	0.61	0.30	0.97

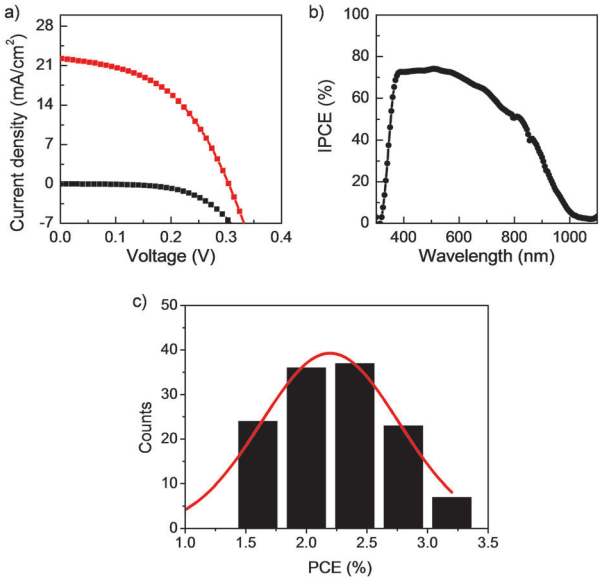

Figure 4. a) *J–V* curve under light (■) and dark (■) conditions and b) IPCE spectrum of the most efficient cell that was prepared in this study. c) Histogram of device efficiencies for the 135 devices that were fabricated independently.

To optimize the cell performance based on experimentally revealed facts, we varied various experimental parameters, such as the blocking-layer thickness, the Sb_2Se_3 loading amount, the temperature of thermal decomposition, the HTM species, and the annealing time. The effects of some of these essential parameters on the device performance are presented in Figure S3–S5. The *J–V* curves and the IPCE spectrum of the most efficient solar cell among the 135 devices that were studied is presented in Figure 4. The device was prepared by repeating a cycle of spin coating a SSP solution (0.05 g mL^{-1}) and thermal decomposition at 150 °C 15 times, followed by crystallization at 300 °C in Ar atmosphere for five minutes. PCPDTBT and phenyl-C_{60}-butyric acid methyl ester ($PC_{60}BM$) (PCPDTBT/PCBM = 15 mg:5 mg in 1 mL of 1,2-dichlorobenzene) were used as the HTM. This device exhibited a J_{SC} value of 22.3 mA cm^{-2}, a V_{OC} value of 304.5 mV, and a *FF* of 47.2%, which corresponds to a PCE of 3.21% under standard illumination conditions (100 mW/cm^2) of air mass 1.5 global (AM 1.5 G). It should be noted that its IPCE spectrum not only dominates the entire visible region, but also expands into the near-IR region up to 1050 nm (Figure 4b). Furthermore, the statistically processed J_{SC} value of 21.8 mA cm^{-2}, which was obtained by integrating the IPCE data with the reference spectrum at AM = 1.5 G, is in good agreement with our experimentally determined results. An additional histogram of PCE for all the independently fabricated cells that contributed to our study is presented in Figure 4c. An evaluation of the available results allowed us to conclude that the multiple-cycle approach provides a simple and effective method for synthesizing highly efficient solar cells utilizing Sb_2Se_3 as the light sensitizer.

In summary, we have achieved a PCE of 3.2% with Sb_2Se_3-based inorganic–organic heterojunction solar cells; Sb_2Se_3 was deposited on mp-TiO_2 by simple multiple cycles of spin coating of a Se-SSP solution and thermal decomposition, followed by annealing at 300 °C in argon atmosphere. The cell presented herein is the first of its kind to use Sb_2Se_3 as an effective light sensitizer, and its capability of expanding its regime to the near-IR region up to 1050 nm was demonstrated. We believe that this unique yet versatile approach represents a powerful method for the fabrication of efficient photovoltaic devices that utilize antimony chalcogenides as the light sensitizer. Our future work will be aimed at improving the performance of Sb_2Se_3-sensitized solar cells, with a focus on the enhancement of V_{oc} value, which was found to be much lower than expected in this study.

Received: September 24, 2013
Published online: December 11, 2013

Keywords: antimony · mesoporous materials · organic–inorganic hybrid composites · selenium · solar cells

[1] a) J. A. Chang, J. H. Rhee, S. H. Im, Y. H. Lee, H.-J. Kim, S. I. Seok, *Nano Lett.* **2010**, *10*, 2609–2612; b) S. H. Im, C.-S. Lim, J. A. Chang, Y. H. Lee, N. Maiti, H.-J. Kim, M. K. Nazeeruddin, M. Grätzel, S. I. Seok, *Nano Lett.* **2011**, *11*, 4789–4793; c) J. A.

Chang, S. H. Im, Y. H. Lee, H.-J. Kim, C.-S. Lim, J. H. Heo, S. I. Seok, *Nano Lett.* **2012**, *12*, 1863 – 1867.
[2] M. Y. Versavel, J. A. Haber, *Thin Solid Films* **2007**, *515*, 7171 – 7176.
[3] P. P. Boix, Y. H. Lee, F. Fabregat-Santiago, S. H. Im, I. Mora-Sero, J. Bisquert, S. I. Seok, *ACS Nano* **2012**, *6*, 873 – 880.
[4] a) C. E. Patrick, F. Giustino, *Adv. Funct. Mater.* **2011**, *21*, 4663 – 4667; b) M. R. Filip, C. E. Patrick, F. Giustino, *Phys. Rev. B* **2013**, *87*, 205125.
[5] W. Shockley, J. Queisser, *J. Appl. Phys.* **1961**, *32*, 510 – 519.
[6] R. N. Bhattacharya, P. Pramanik, *Sol. Energy Mater.* **1982**, *6*, 317 – 322.
[7] N. Guijarro, T. Lutz, T. Lana-Villarreal, F. O'Mahony, R. Gómez, S. A. Haque, *J. Phys. Chem. Lett.* **2012**, *3*, 1351 – 1356.
[8] Y. Rodríguez-Lazcano, Y. Peña, M. T. S. Nair, P. K. Nair, *Thin Solid Films* **2005**, *493*, 77 – 82.
[9] S. M. Pawar, B. S. Pawar, J. H. Kim, O.-S. Joo, C. C. Lokhande, *Curr. Appl. Phys.* **2011**, *11*, 117 – 161.
[10] N. Maiti, S. H. Im, C.-S. Lim, S. I. Seok, *Dalton Trans.* **2012**, *41*, 11569 – 11572.
[11] P. Patnaik, *Handbook of Inorganic Chemicals*, McGraw-Hill, New York, **2002**.
[12] N. Maiti, S. H. Im, Y. H. Lee, C.-H. Kim, S. I. Seok, *CrystEngComm* **2011**, *13*, 3767 – 3772.

